

Supplemental material

Kruse et al., <https://doi.org/10.1083/jcb.201802076>

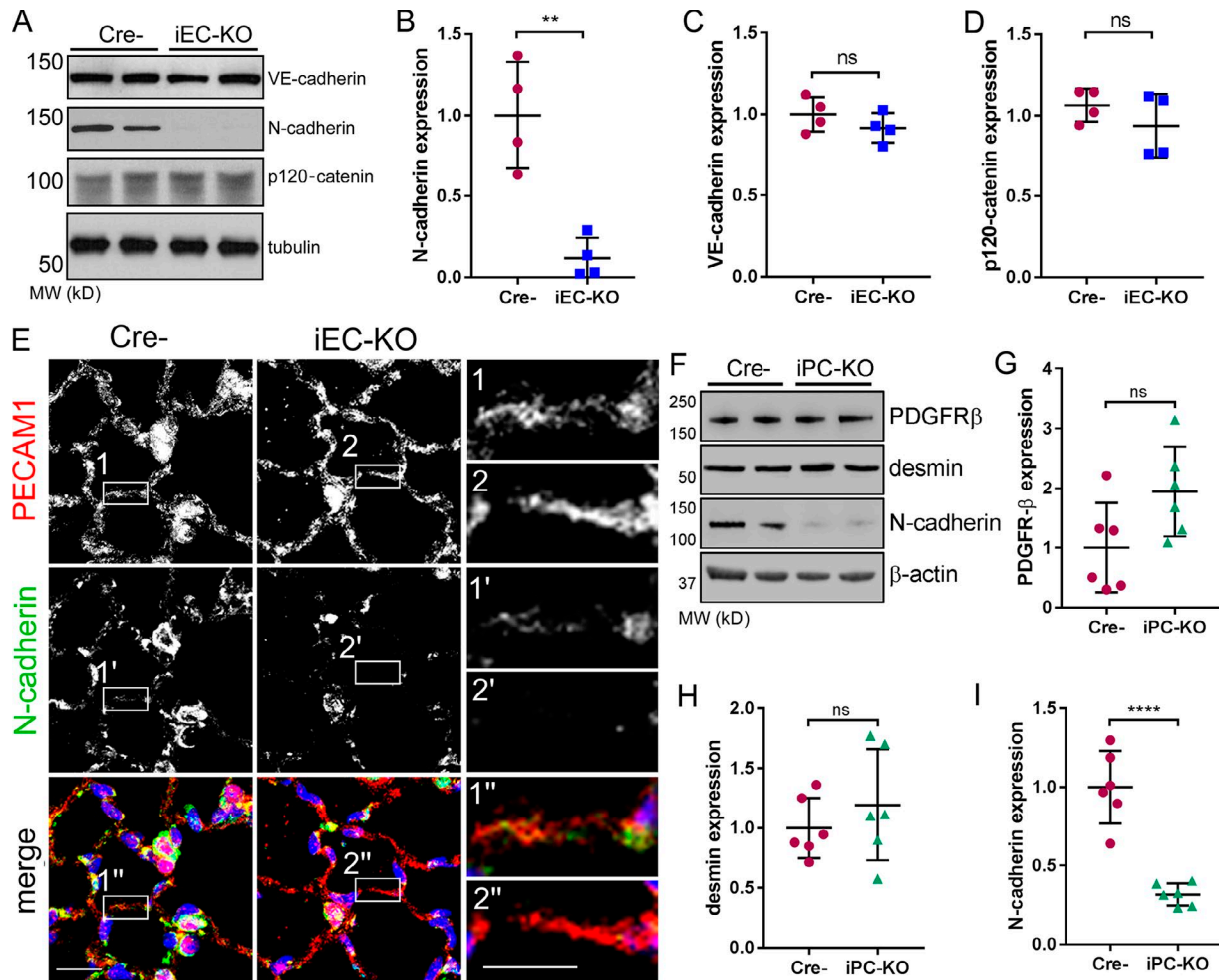


Figure S1. **Genetic deletion of N-cadherin in ECs or pericytes induces vascular leakage.** Related to Fig. 1. **(A)** Western blot analysis of endothelial specific fractions collected from lungs of *Cre*⁻ and *Cdh2* iEC-KO littermates for N-cadherin, VE-cadherin, p120-catenin, and tubulin. **(B-D)** Quantification of N-cadherin (B), VE-cadherin (C), and p120-catenin (D) expression in ECs normalized to *Cre*⁻ mice using data in A; *n* = 4 mice per group. **, *P* < 0.01, a two-tailed, unpaired *t* test was used to test significance. **(E)** Representative confocal images of mouse lung sections from *Cre*⁻ and *Cdh2* iEC-KO mice stained for N-cadherin (green on merged image), PECAM1 (red), and nuclei (DAPI, blue); enlarged insets from each panel are indicated by 1, 1', or 1'' for control and 2, 2', and 2'' for iEC-KO mice. Bars, 10 μm; insets, 5 μm. Note reduced expression of N-cadherin in PECAM1-positive cells of *Cdh2* iEC-KO mice. **(F)** Western blot analysis of pericytes isolated from *Cre*⁻ and *Cdh2* iPC-KO littermates for N-cadherin, PDGFRβ, desmin, and β-actin. **(G-I)** Quantification of expression levels of PDGFRβ (G), desmin (H), and N-cadherin (I) in brain pericytes normalized to *Cre*⁻ mice using data in F; *n* = 6 samples from three mice per group. ****, *P* < 0.0001, a two-tailed, unpaired *t* test. (B-D and G-I) Data are shown as mean ± SD.

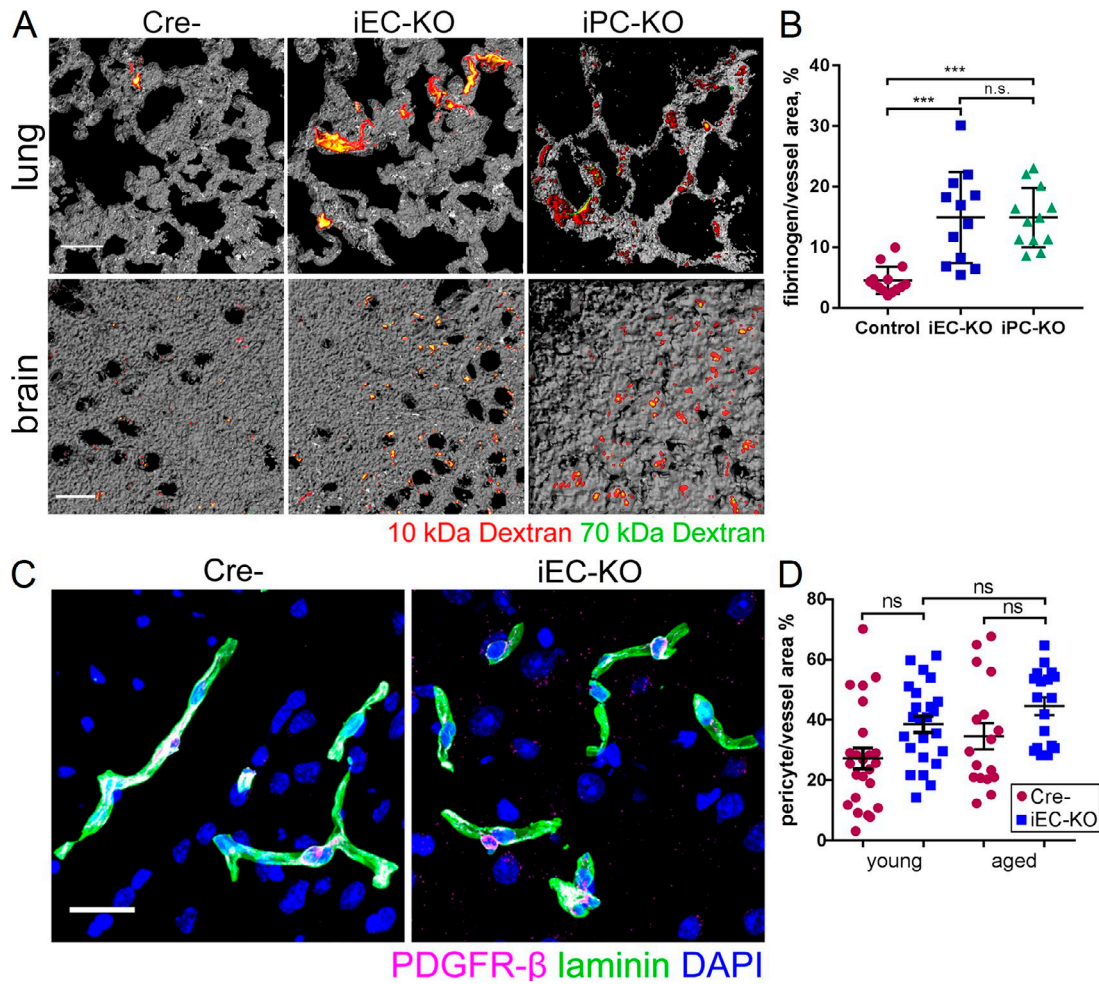


Figure S2. **Genetic deletion of N-cadherin in ECs or pericytes induces vascular leakage.** Related to Fig. 1. **(A)** 3D reconstructed images of mouse lung and brain tissue from Cre⁻ control, *Cdh2* iEC-KO, and *Cdh2* iPC-KO mice after injection of 10-kD dextran (red) and 70-kD dextran (green); Bar, 10 μ m. Tissue architecture from autofluorescence is shown in gray. **(B)** Measurement of lung transvascular leakage of fibrinogen in Cre⁻ control, *Cdh2* iEC-KO, and *Cdh2* iPC-KO mice. The leakage is expressed as a percent of fibrinogen-positive vessel area. $n = 12$ – 16 fields from three to five mice per group. ***, $P < 0.001$, ANOVA with Tukey's post hoc test. Data are shown as mean \pm SD. **(C)** Representative confocal images of mouse brain sections from Cre⁻ and *Cdh2* iEC-KO mice stained for PDGFR- β (green), laminin (magenta), and nuclei (DAPI, blue). Bar, 10 μ m. **(D)** Quantification of pericyte coverage of brain microvessels expressed as pericyte area per vessel area (PDGFR- β /laminin) in young adult (12–18-wk-old) and aged (36–40-wk-old) mice. $n = 24$ fields from three to four mice per group. ns, ANOVA with Tukey's post hoc test. Data are shown as mean \pm SEM.

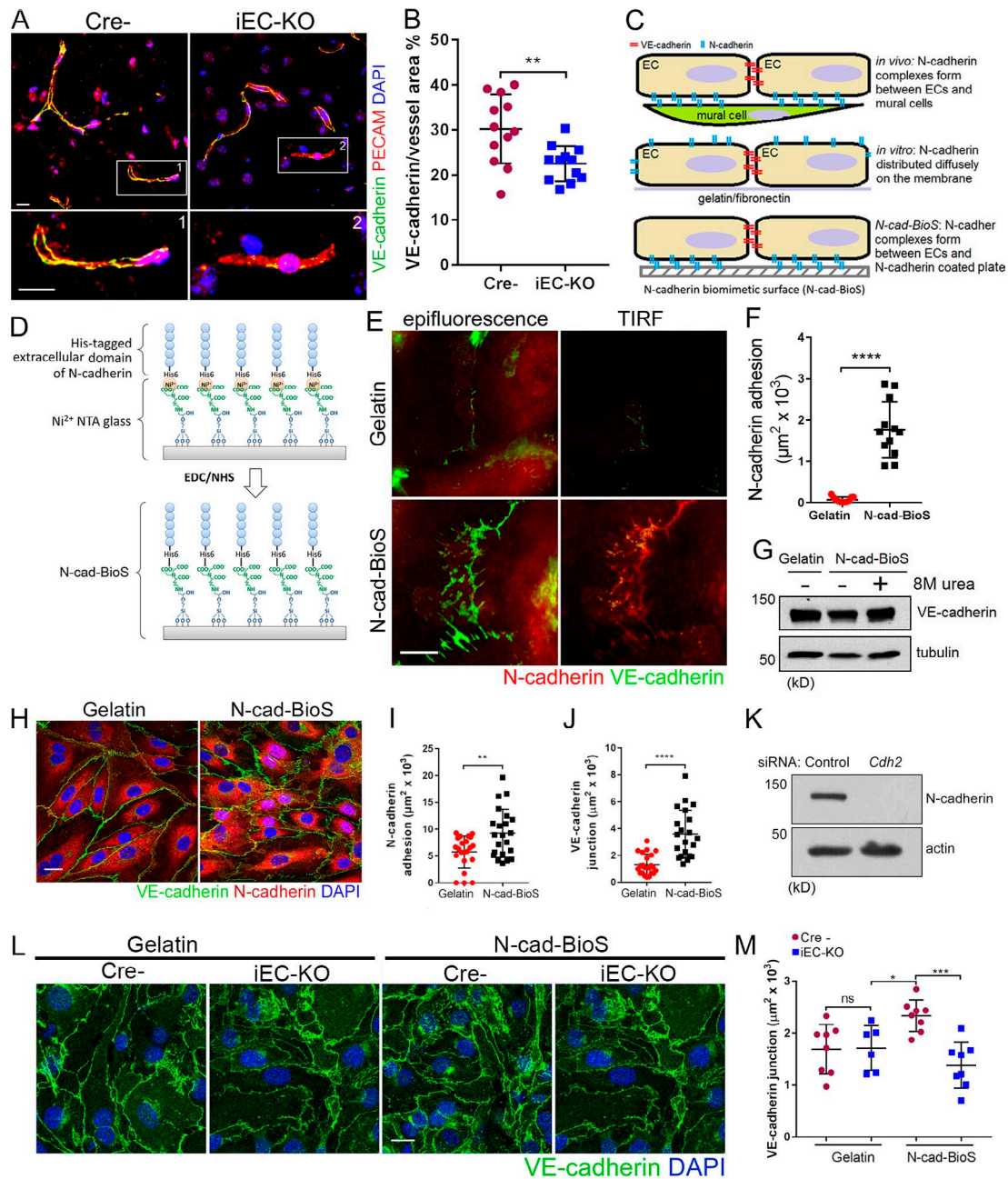


Figure S3. Genetic deletion of N-cadherin disassembles VE-cadherin adhesion. Related to Fig. 2. **(A)** Representative confocal images of mouse brain sections from Cre⁻ and *Cdh2* iEC-KO mice stained for VE-cadherin (green), PECAM1 (red), and nuclei (DAPI, blue); enlarged insets for merged images are shown below and labeled as indicated. Bar, 10 μ m; insets, 5 μ m. VE-cadherin at PECAM1-positive junctions is reduced in *Cdh2* iEC-KO mice as compared with controls. **(B)** VE-cadherin adhesion area normalized to PECAM1 area from images in A. $n = 12$ images from three mice per group. **, $P < 0.01$, a two-tailed, unpaired t test was used to test significance. **(C)** Model depicting N-cadherin localization in ECs *in vivo*, *in vitro*, and on biomimetic surface. Gelatin versus N-cad-BioS is shown for a cell culture model. **(D)** Schematic representation of steps used to manufacture N-cad-BioS. The His-tagged extracellular domain of N-cadherin is covalently linked to Ni-NTA glass to allow similar orientation of all molecules. See Materials and methods. **(E)** Immunofluorescent staining of HPAEC monolayers for VE- (green) and N-cadherin (red) proteins. Side-by-side comparison of epifluorescent and TIRF images demonstrates clustering of N-cadherin at abuminal side of the cells in HPAECs grown on N-cad-BioS but not on gelatin. Bar, 10 μ m. Note VE-cadherin is excluded from N-cadherin adhesion. **(F)** Quantification of N-cadherin adhesion area from images in (E). $n = 12$ –15 images per group from three independent experiments. ****, $P < 0.0001$, a two-tailed, unpaired t test. **(G)** Western blot analysis of VE-cadherin and β -tubulin (loading control) in HPAECs grown on gelatin, N-cad-BioS, or N-cad-BioS denatured with 8 M urea. Note there is no change in VE-cadherin level. **(H)** Confocal images of VE-cadherin (green), N-cadherin (red), and nuclei (DAPI, blue) in human lung microvascular endothelial cells grown on either gelatin or N-cad-BioS. Bar, 10 μ m. **(I and J)** Quantification of N-cadherin (I) and VE-cadherin (J) adhesion area from cells in H. $n = 22$ images per group from three independent experiments. **, $P < 0.01$; ****, $P < 0.0001$, a two-tailed, unpaired t test. **(K)** Western blot analysis of N-cadherin expression in HPAECs treated with *Cdh2* or control (scrambled) siRNA; β -actin is used as a loading control. **(L)** Confocal images of VE-cadherin (green) and nuclei (DAPI, blue) in murine ECs isolated from lungs of Cre⁻ or *Cdh2* iEC-KO mice and grown on either gelatin or N-cad-BioS. Bar, 10 μ m. **(M)** Quantification of VE-cadherin adhesion area from images in K. $n = 6$ –8 images per group. *, $P < 0.05$; ***, $P < 0.001$, ANOVA with Tukey's post hoc test. (B, F, I, J, and M) Data are shown as mean \pm SD.

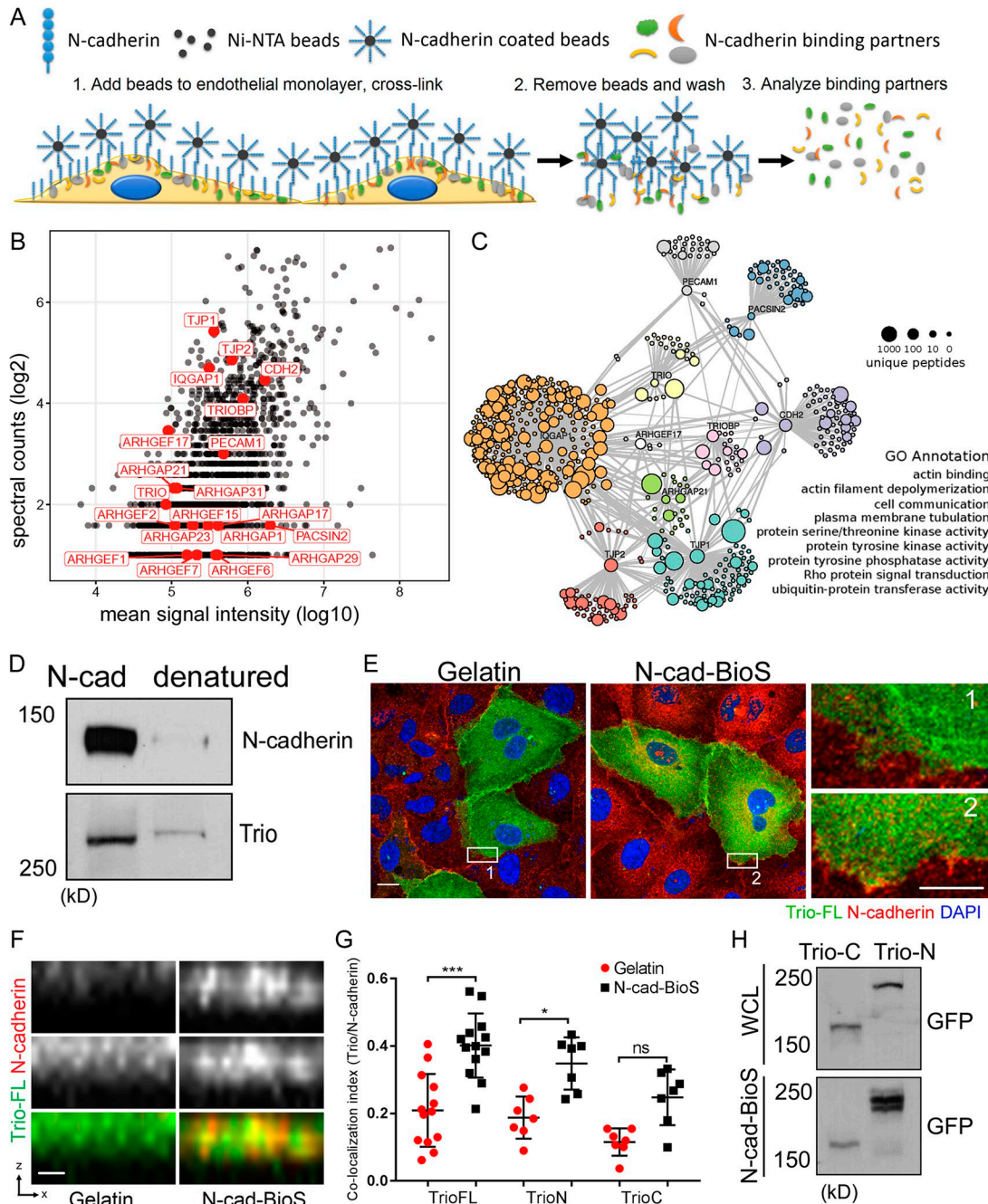


Figure S4. **N-cadherin complexed with Trio signals assembly of VE-cadherin adhesion.** Related to Fig. 4. **(A)** Schematic representation of the method used for isolation of N-cadherin adhesion complex. The His-tagged extracellular domain of N-cadherin is covalently linked to Ni²⁺-NTA beads. N-cad-BioS beads are added to the endothelial monolayer and allowed to form N-cadherin adhesion complex, which was cross-linked to the beads with the thiol-reversible cross-linker, DTSP. Beads were washed to remove contaminating proteins and cross-link was reversed using DTT. Proteins were then separated by SDS-PAGE and submitted for mass spectrometry analysis. **(B and C)** Proteins of N-cadherin adhesion complex detected by mass spectrometry. (B) Scatter plot of mean intensity versus spectral counts. (C) Interaction network for proteins of interest highlighted in B with clusters established based on individual protein interaction profiles; see Materials and methods. GO associations were based on a hypergeometric test ($P < 1e^{-12}$). **(D)** Western blot analysis of isolated N-cadherin adhesion complex for endogenous N-cadherin and Trio proteins. HPAECs were incubated with either N-cad-BioS beads or denatured N-cad-BioS beads for 1 h; N-cadherin complex was collected and processed as described in Methods. **(E and F)** Confocal lateral (E, insets) and axial (F) images of exogenously expressed FL GFP-Trio. Cells were stained for N-cadherin (red) and nuclei (DAPI; blue). Enlarged insets are shown on right; bar, 10 μ m for lateral; insets, 5 μ m; 1 μ m for axial. **(G)** Colocalization coefficient of N-cadherin clusters with GFP-Trio-FL (shown in E), GFP-Trio-N (N terminus), and GFP-Trio-C (C terminus). The colocalization index was calculated as the sum of positive pixels for both N-cadherin and Trio divided by the total number of N-cadherin-positive pixels. $n = 7-13$ cells per condition from three independent experiments. *, $P < 0.05$; ****, $P < 0.0001$, a two-tailed, unpaired t test. Data are shown as mean \pm SD. **(H)** Western blot analysis of GFP-Trio deletion mutants expressed in ECs; whole cell lysates (WCLs) and isolated N-cadherin complexes (N-cad-BioS) indicate preferential recruitment of GFP-Trio-N to N-cadherin complexes.

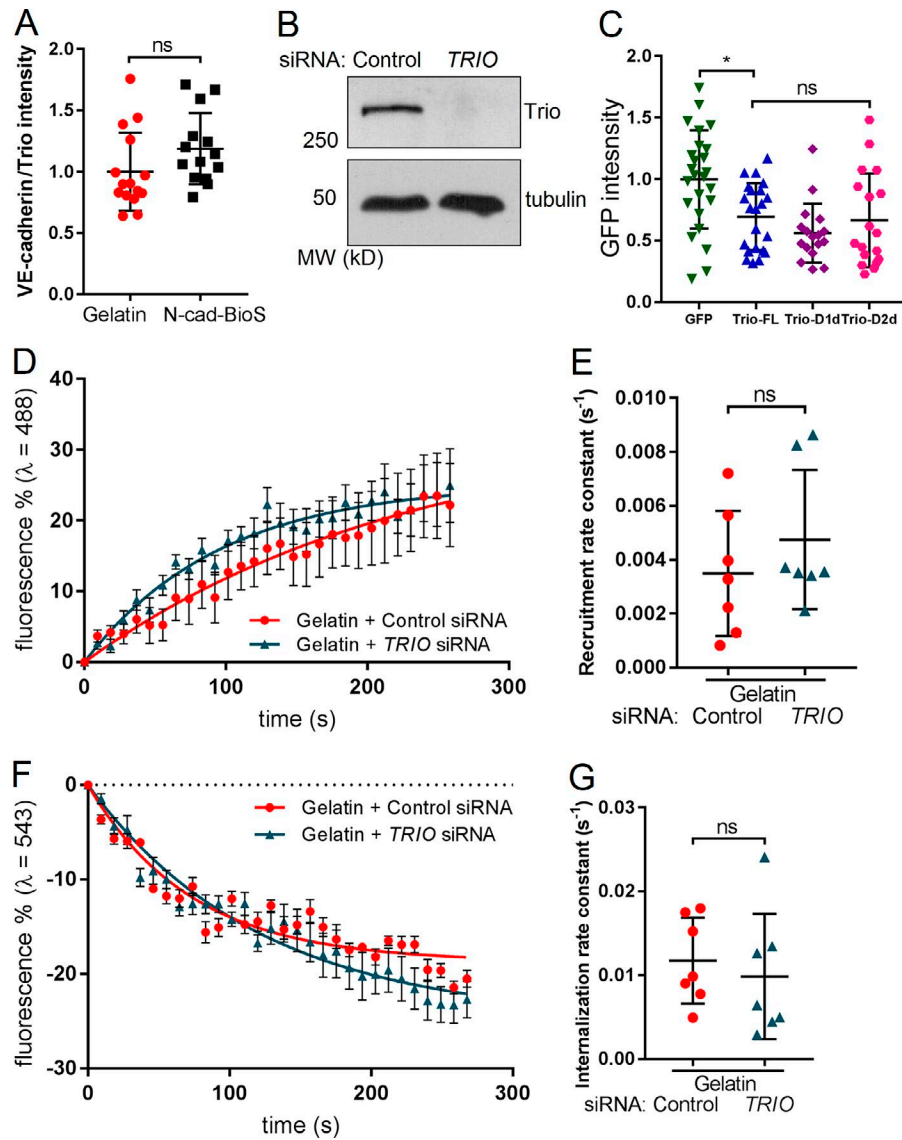


Figure S5. **N-cadherin complexed with Trio signals assembly of VE-cadherin adhesion.** Related to Fig. 4. **(A)** VE-cadherin fluorescent intensity normalized to Trio fluorescent intensity at AJs in cells expressing GFP-Trio-FL and stained with VE-cadherin. Accumulation of Trio at VE-cadherin junctions is not regulated by N-cadherin signaling. $n = 15$ cells per condition from three independent experiments. ns, a two-tailed, unpaired t test. **(B)** Western blot analysis of Trio expression after treatment of HPAECs with control or *TRIO* siRNA. β -Tubulin was used as a loading control. **(C)** Normalized ratio of GFP fluorescent intensity from cells expressing GFP, GFP-Trio-FL, and GFP-Trio mutants from cells analyzed in Fig. 5 C. *, $P < 0.05$, ANOVA with Tukey's post hoc test. **(D and E)** The rates of VE-cadherin recruitment to AJs (D) and the recruitment rate constants (E) in cells grown on gelatin after depletion of Trio or treatment with control siRNA; $n = 7$ junctions per group from three independent experiments. ns, a two-tailed, unpaired t test. **(F and G)** Rates of VE-cadherin internalization from AJs (F) and internalization rate constants (G) in cells grown on gelatin after depletion of Trio or treatment with control siRNA; $n = 7$ junctions per group from three independent experiments; ns, a two-tailed, unpaired t test. (A, C, E, and G) Data are shown as mean \pm SD. (D and F) Data are shown as mean \pm SEM.

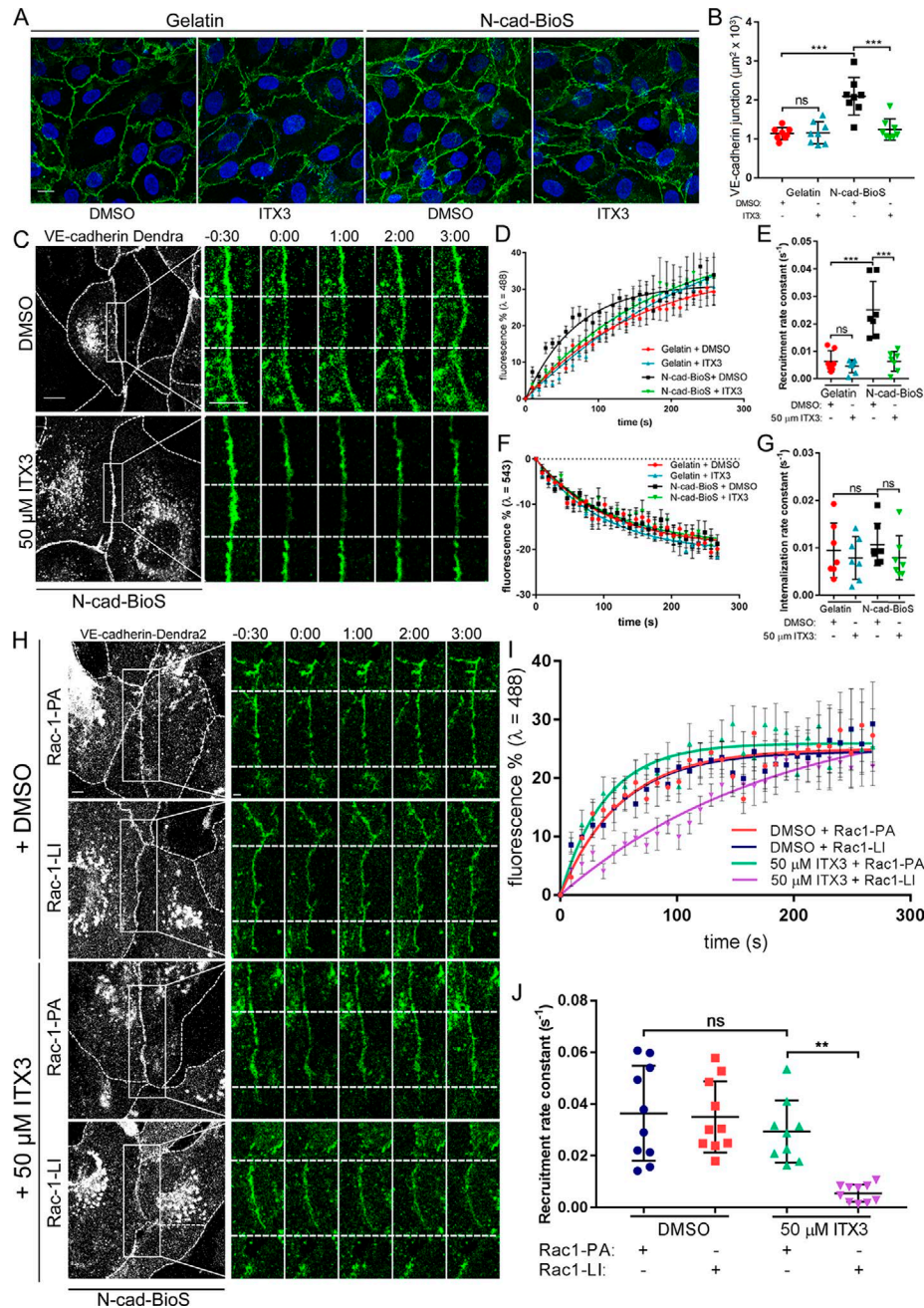


Figure S6. **Trio GEF1 activity is required for assembly of VE-cadherin junctions downstream of N-cadherin signaling.** Related to Figs. 5, 6, and 7. **(A)** Confocal images of HPAECs grown on either gelatin or N-cad-BioS and treated with vehicle (DMSO) or 50 μM ITX3 to inhibit the interaction of Trio with Rac1. Cells were stained for VE-cadherin (green) and nuclei (DAPI, blue). Bar, 10 μm . **(B)** Quantification of VE-cadherin junction area using images in A. Note inhibition of Trio GEF1 significantly reduced the density of VE-cadherin at AJs only in cells grown on N-cad-BioS. $n = 8$ images per group from three independent experiments. *******, $P < 0.001$, ANOVA with Tukey's post hoc test. **(C)** Time-lapse images of VE-cadherin–Dendra2 before and after photo-conversion at $t = 0$ within the irradiation zone (indicated by area between dashed lines on insets) in HPAECs grown on N-cad-BioS after treatment with vehicle (DMSO) or 50 μM ITX3. Dashed lines of grayscale images outline the cell borders. Bar, 5 μm . **(D and E)** The rates of VE-cadherin recruitment to AJs (D) and recruitment rate constants (E) in cells grown on gelatin or N-cad-BioS after treatment with vehicle (DMSO) or 50 μM ITX3; $n = 7$ junctions per group from three independent experiments. *******, $P < 0.001$, ANOVA with Tukey's post hoc test. **(F and G)** Rates of VE-cadherin internalization from AJs (F) and internalization rate constants (G) in cells grown on gelatin or N-cad-BioS after treatment with vehicle (DMSO) or 50 μM ITX3; $n = 7$ junctions per group from three independent experiments. ns, ANOVA with Tukey's post hoc test. **(H)** Time-lapse images of VE-cadherin–Dendra2 in cells coexpressing either CFP-tagged PA-Rac1 or LI-Rac1 before and after photo-conversion of Dendra2 at $t = 0$ within the irradiation zone (indicated by area between dashed lines on insets) in HPAECs grown on N-cad-BioS after treatment with vehicle (DMSO) or 50 μM ITX3. Dashed lines outline the cell borders in grayscale images. Bar, 5 μm ; insets, 2 μm . PA-Rac1 was activated with $\lambda = 458$ nm within the photo-conversion zone. Bars, 5 μm ; insets, 2 μm . **(I and J)** The rates of VE-cadherin recruitment to AJs (I) and recruitment rate constants (J) in cells grown on N-cad-BioS after treatment with vehicle (DMSO) or 50 μM ITX3, and after activation of PA-Rac1 or LI-Rac1; $n = 7$ junctions per group from three independent experiments. ******, $P < 0.01$, ANOVA with Tukey's post hoc test. PA-Rac1 rescues VE-cadherin recruitment rate in cells treated with ITX3. (B, D, E–G, I, and J) Data are shown as mean \pm SD.

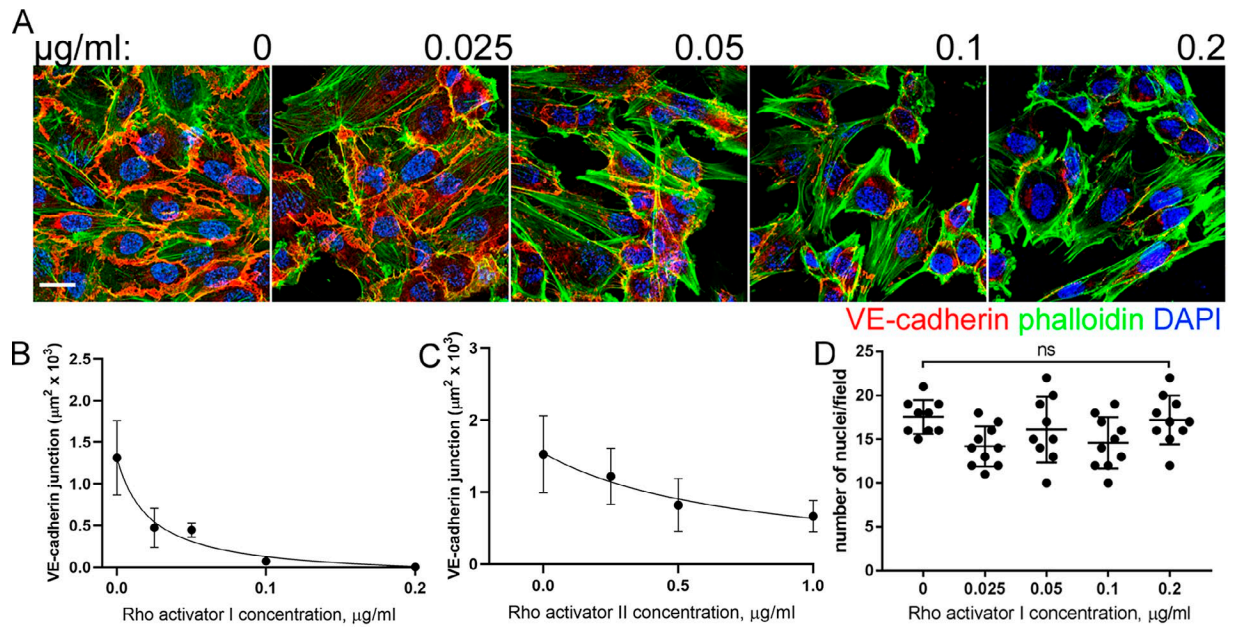


Figure S7. **Activation of RhoA and increased intracellular tension are not sufficient to induce assembly of VE-cadherin junctions.** (A) Confocal images of HPAECs grown on gelatin and stained for VE-cadherin (red), F-actin (phalloidin, green), and DAPI. Cells were treated with indicated doses of Rho activator I. Bar, 10 µm. We observed formation of actin stress-fibers and destabilization of VE-cadherin junctions with increased concentration of Rho activator I. (B and C) Quantification of VE-cadherin area from images in A for different doses of Rho activator I (B) and Rho activator II (C). *n* = 8–10 fields of view from two independent experiments. (D) Quantification of number of nuclei per field for images in A. Number of nuclei per field did not change with increasing concentrations of Rho activator I. *n* = 8–10 fields of view from two independent experiments. ns, ANOVA with Tukey’s post hoc test. (B–D) Data are shown as mean ± SD.

Table S4. All information regarding reagents and tools used in the paper

Reagent or resource	Source	Identifier
Antibodies		
Goat polyclonal anti-VE-cadherin	Santa Cruz	sc-6458
Rabbit polyclonal anti-VE-cadherin	Cell Signaling Technology	#2158
Rat monoclonal anti-VE-cadherin	BD Biosciences	555289
Rabbit polyclonal anti-N-cadherin	Santa Cruz	sc-7939
Rabbit polyclonal anti-N-cadherin	Abcam	ab12221
Mouse monoclonal anti-N-cadherin	ECM Biosciences	CM-1701
Rabbit polyclonal anti-N-cadherin	Abcam	ab76057
Rabbit polyclonal anti-Desmin	Abcam	ab15200
Rat polyclonal anti-CD31	BD Bioscience	#550274
Rabbit polyclonal anti-CD31	Abcam	ab28364
Rabbit polyclonal anti-CD31	Santa Cruz	sc-1506-R
Rabbit polyclonal anti-Laminin	Abcam	ab11575
Rabbit polyclonal anti-Fibrinogen	Dako	A0080
Mouse monoclonal anti- β -actin	Proteintech	60008-1-Ig
Mouse monoclonal anti- β -actin - Peroxidase	Sigma-Aldrich	A3854
Alexa Fluor 488 Phalloidin	Invitrogen	A12379
Mouse monoclonal anti- β -tubulin	Sigma-Aldrich	T8328
Goat polyclonal anti-PDGFR β Antibody	R & D Systems, Inc.	AF1042
Rabbit polyclonal anti Trio antibody	Bethyl Laboratories	A304-269A-T
Rabbit polyclonal anti Trio lantibody	Santa Cruz	sc-28564
Rabbit polyclonal Phospho-Myosin Light Chain 2 (Ser 19) antibody	Cell Signaling Technology	#3671
Bacterial and Virus Strains		
VE-cadherin-Dendra2 adenovirus	Daneshjou et al., 2015	NA
MAX Efficiency DH5 α Competent Cells	Thermo Fisher Scientific	18258012
One Shot™ BL21(DE3) Chemically Competent <i>E. coli</i>	Thermo Fisher Scientific	C600003
Chemicals, Peptides, and Recombinant Proteins		
Recombinant human N-cadherin-His	Sino Biological	11039-H08H
Recombinant human N-cadherin-Fc-His	Sino Biological	11039-H03H
EDC	Thermo Fisher Scientific	22980
EDTA	Research Products International	E57020
Imidazole	Sigma-Aldrich	I5513
N-Hydroxysuccinimide	Sigma-Aldrich	130672
Glymo	Sigma-Alrich	440167
AB-NTA (free acid)	Dojindo	A459-10
10 kD Dextran, Alexa Fluor 555	Sigma-Aldrich	D34679
70 kD Dextran, Oregon Green 488	Sigma-Aldrich	D7173
NiCl ₂	Thermo Fisher Scientific	N53-500
DSP (dithiobis(succinimidyl propionate))	Thermo Fisher Scientific	22585
DL-Dithiotreitol	Sigma-Aldrich	D0632
4 \times Laemmli buffer	BioRad	1610747
RIPA	Sigma-Aldrich	R0278
ITX3	Millipore	645890
HisPur Ni-NTA Magnetic Beads	Thermo Fisher Scientific	88831

Table S4. All information regarding reagents and tools used in the paper (Continued)

Reagent or resource	Source	Identifier
Fibronectin	Sigma-Aldrich	F1141
Fibronectin	Sigma-Aldrich	F0895
Laminin	Sigma-Aldrich	L2020
Collagen type 1	Sigma-Aldrich	C8919
Glass cover slips	Schott Nexterion	1472309
¹²⁵ I radiolabeled human serum albumin, 10 uCi/ml	Anazao Health	I-125 HSA
Vectashield	Vector Laboratories, Inc.	H-1000
Prolong Gold Antifade	Thermo Fisher Scientific	P36930
Fluoromount	Southern Biotech	0100-01
Rho Kinase Inhibitor III, Rockout	Santa Cruz	sc-203237
Rho Activator I	Cell Signaling	CN01-A
Rho Activator II	Cell Signaling	CN03-A
BSA, Alexa Fluor 647 conjugate	Thermo Fisher Scientific	A34785
Critical Commercial Assays		
Basic Endothelial Cells Nucleofector Kit	Lonza	VPI-1001
GeneSilencer Transfection Reagent	Genlantis	T500020
Lipofectamine 2000 Transfection Reagent	Thermo Fisher Scientific	11668019
RhoA G17A Agarose Beads	Abcam	Ab211183
Experimental Models: Cell Lines		
Human Pulmonary Aortic Endothelial cells	Lonza	CC-2530
Experimental Models: Organisms/Strains		
N-cadherin-flox/flox	Jackson	B6.129S6(SJL)-Cdh2tm1Glr/J
end-SCL-CreERT ²	Göthert et al., 2004	Available from Jackson, Tg(Tal1-cre/ERT)42-056Jrg
PDGFRb-P2A-CreERT ²	Cuervo et al., 2017	Available from Jackson, B6.Cg-Pdgfrbtm1.1(cre/ERT2)Csln/J
N-cadherin-flox/flox- SCL-CreERT2	This paper	NA
N-cadherin-flox/flox- PDGFRb-P2A-CreERT2	This paper	NA
Oligonucleotides		
<i>Cdh2</i> ON-TARGETplus siRNA Target Sequence: GUGCAACAGUAUACGUUAA	Dharmacon	J-011605-06
<i>Cdh2</i> ON-TARGETplus siRNA Target Sequence: GGACCCAGAU CGAUUAUUG	Dharmacon	J-011605-07
<i>Cdh2</i> ON-TARGETplus siRNA Target Sequence: CAUAGUAGCUAAUUAACU	Dharmacon	J-011605-08
<i>Cdh2</i> ON-TARGETplus siRNA Target Sequence: GACAGCCUCUUCUCAUUGU	Dharmacon	J-011605-09
<i>TRIO</i> ON-TARGETplus siRNA Target Sequence: GUAAAGAAGUGAAAGAUUC	Dharmacon	J-005047-05
<i>TRIO</i> ON-TARGETplus siRNA Target Sequence: CGACCUAUCCGUAGCAUUA	Dharmacon	J-005047-06
<i>TRIO</i> ON-TARGETplus siRNA Target Sequence: GGAAUACAACCACGAAGAA	Dharmacon	J-005047-07
<i>TRIO</i> ON-TARGETplus siRNA Target Sequence: AGAACAGGUUUGCAUUA	Dharmacon	J-005047-08
<i>SMARTpool</i> : ON-TARGETplus <i>CDH5</i> siRNA:Combination of four Target Sequences:	Dharmacon	L-003641-00-0005
GGACAUACACCACGAAAC		J-003641-06
GAGCCCAGGUCAUUAUCAA		J-003641-07
CGAUAAUUCUGGACGUUU		J-003641-08
UGACGUGGAUUACGACUUC		J-003641-09
Recombinant DNA		
pTriEx-mCerulean-PA-Rac1	Wu et al., 2009	Addgene: 22030
pTriEx-PA-Rac1-C450A	Wu et al., 2009	Addgene: 22025

Table S4. All information regarding reagents and tools used in the paper (Continued)

Reagent or resource	Source	Identifier
peGFP[C1] Trio-FL	van Rijssel et al., 2012	N/A
peGFP[C1] Trio-N	van Rijssel et al., 2012	N/A
peGFP[C1] Trio-C	van Rijssel et al., 2012	N/A
pTriEx-Rac1 FLARE.dc Biosensor WT	MacNevin et al., 2016	N/A
pTriEx-RhoA FLARE.sc Biosensor WT	Pertz et al., 2006	Addgene: 12150
GFP-Trio-D1d	Cannet et al., 2014	N/A
GFP-Trio-D2d	Cannet et al., 2014	N/A
pGEX-4T1-Rac1 G15A	García-Mata et al., 2006	N/A
Software and Algorithms		
ImageJ (Fiji)	National Institutes of Health	https://fiji.sc/
Metamorph	Olympus	https://www.olympus-lifescience.com/en/software/metamorph/
Zen	Carl Zeiss	https://www.zeiss.com/microscopy/us/products/microscope-software/zen-lite.html
Prism 7	GraphPad	https://www.graphpad.com/scientific-software/prism/
Photoshop CS6	Adobe	http://www.adobe.com/products/photoshop.html
R	The R Project for Statistical Computing	https://www.r-project.org/

Provided online are three tables. Table S1 shows a summary by gene names for peptides identified in N-cadherin MS experiment after removing non-unique peptides. Only proteins with greater than three unique peptides and mean peptide intensities (log₁₀) greater than six were included. Table S2 shows proteins detected in N-cadherin MS (from Table S1), the log₁₀ mean intensity score, and the spectral counts were used to create GO clusters based on known interactions. GO terms were obtained from BioMart, and associations were computed using the hypergeometric test ($n > 5$) for each of the nine clusters containing the proteins of interest. Table S3 shows previously known protein interaction scores summarized by gene names (based on HIPPIE dataset; see Materials and methods). For each gene of interest selected, the protein interaction score (0–1) was calculated. Protein interactions were filtered to include only those with confidence scores greater than 0.2.

References

- Cannet, A., S. Schmidt, B. Delaval, and A. Debant. 2014. Identification of a mitotic Rac-GEF, Trio, that counteracts MgcRacGAP function during cytokinesis. *Mol. Biol. Cell.* 25:4063–4071. <https://doi.org/10.1091/mbc.e14-06-1153>
- Cuervo, H., B. Pereira, T. Nadeem, M. Lin, F. Lee, J. Kitajewski, and C.S. Lin. 2017. PDGFR β -P2A-CreER^{T2} mice: a genetic tool to target pericytes in angiogenesis. *Angiogenesis.* 20:655–662. <https://doi.org/10.1007/s10456-017-9570-9>
- Daneshjou, N., N. Sieracki, G.P. van Nieuw Amerongen, D.E. Conway, M.A. Schwartz, Y.A. Komarova, and A.B. Malik. 2015. Rac1 functions as a reversible tension modulator to stabilize VE-cadherin trans-interaction. *J. Cell Biol.* 208:23–32. <https://doi.org/10.1083/jcb.201409108>
- García-Mata, R., K. Wennerberg, W.T. Arthur, N.K. Noren, S.M. Ellerbroek, and K. Burridge. 2006. Analysis of activated GAPs and GEFs in cell lysates. *Methods Enzymol.* 406:425–437. [https://doi.org/10.1016/S0076-6879\(06\)06031-9](https://doi.org/10.1016/S0076-6879(06)06031-9)
- Göthert, J.R., S.E. Gustin, J.A. van Eekelen, U. Schmidt, M.A. Hall, S.M. Jane, A.R. Green, B. Göttgens, D.J. Izon, and C.G. Begley. 2004. Genetically tagging endothelial cells in vivo: bone marrow-derived cells do not contribute to tumor endothelium. *Blood.* 104:1769–1777. <https://doi.org/10.1182/blood-2003-11-3952>
- MacNevin, C.J., A. Touthkine, D.J. Marston, C.W. Hsu, D. Tsygankov, L. Li, B. Liu, T. Qi, D.V. Nguyen, and K.M. Hahn. 2016. Ratiometric Imaging Using a Single Dye Enables Simultaneous Visualization of Rac1 and Cdc42 Activation. *J. Am. Chem. Soc.* 138:2571–2575. <https://doi.org/10.1021/jacs.5b09764>
- Pertz, O., L. Hodgson, R.L. Klemke, and K.M. Hahn. 2006. Spatiotemporal dynamics of RhoA activity in migrating cells. *Nature.* 440:1069–1072. <https://doi.org/10.1038/nature04665>
- van Rijssel, J., J. Kroon, M. Hoogenboezem, F.P. van Alphen, R.J. de Jong, E. Kostadinova, D. Geerts, P.L. Hordijk, and J.D. van Buul. 2012. The Rho-guanine nucleotide exchange factor Trio controls leukocyte transendothelial migration by promoting docking structure formation. *Mol. Biol. Cell.* 23:2831–2844. <https://doi.org/10.1091/mbc.e11-11-0907>
- Wu, Y.I., D. Frey, O.I. Lungu, A. Jaehrig, I. Schlichting, B. Kuhlman, and K.M. Hahn. 2009. A genetically encoded photoactivatable Rac controls the motility of living cells. *Nature.* 461:104–108. <https://doi.org/10.1038/nature08241>